[5] M. S. Wang, M. Carriere, P. O'Sullivan, and B. Maoz, "A single-chip MMIC transceiver for 2.4 GHz spread spectrum communications," *IEEE Microwave and Millimeter-Wave Monolithic Circuit Symp.*, pp. 19–22, May 1994.
[6] A. V. Khramov and V. A. Shchelokov, "The design of microwave transistor multipliers," *Radiotekhnica*, no. 9, pp. 23–25, 1987.
[7] A. Z. Venger, A. N. Ermak, and A. M. Yakimeko, "Simple transistor frequency multiplier," *Pribory i Tekhnika Éksperimenta*, no. 3, pp. 143–144, May-June, 1979.
[8] R. H. Johnston and A. R. Boothroyd, "High-frequency transistor frequency multipliers and power amplifiers," *IEEE J. Solid-State Circ.*, vol. SC-7, pp. 81–89, Feb. 1972.
[9] G. D. O'Clock, Jr., and R. J. Dauphinee, "High-gain frequency multipliers," *IEEE Proc. Lett.*, pp. 1363–1365, Sept. 1970.
[10] Héctor J. De Los Santos, Madjid Hafizi, Takyiu Liu, and Dave B. Rensch, "Electron transport mechanisms in abrupt- and graded-base/collector AlInAs/GaInAs/InP double heterostructure bipolar transistors," *1994 Inter. Symp. on Compound Semiconductors*, pp. 645–650, Sept. 1994.
[11] M. Hafizi, T. Liu, P. A. Macdonald, *et al.*, "High-performance microwave power AlInAs/GaInAs/InP double heterojunction bipolar transistors with compositionally graded base/collector junction," in *IEEE Int. Electron Devices Meeting Dig.*, Dec. 1993, pp. 791–794.

Analysis of Slot-Coupled Double-Sided Cylindrical Microstrip Lines

Jui-Han Lu and Kin-Lu Wong

***Abstract*— The problem of double-sided cylindrical microstrip lines coupled through a rectangular slot in the common cylindrical ground plane is studied using the reciprocity theorem and a moment-method calculation. The oretical results of the S parameters for the slot-coupled cylindrical microstrip lines are calculated and analyzed. Experiments are also conducted to verify the theoretical results.**

I. Introduction

Slot-coupled double-sided microstrip lines have recently found applications in the design of directional couplers [1], which are useful for beam-forming networks, multiport amplifiers, and other important microwave and millimeter-wave circuits. Several related studies have also been reported [2]–[4], in which the slot-coupled microstrip lines on a planar geometry are treated. In this paper we present an analysis of the slot-coupled microstrip lines in a cylindrical structure; i.e., the slot-coupled double-sided cylindrical microstrip lines. This new structure is useful for the design of conformal printed circuits on cylindrical surfaces. To perform the analysis we apply the reciprocity theorem and use the exact Green's functions for the grounded cylindrical substrate in a moment-method calculation for the unknown slot electric fields. The formulation of the S parameters for the slot-coupled cylindrical microstrip lines is presented, and theoretical results are calculated and discussed.

Manuscript received August 28, 1995; revised March 20, 1996. This work was supported by the National Science Council of the Republic of China under Grant NSC85-2221-E-110-002.

The authors are with the Department of Electrical Engineering, National Sun Yat-Sen University, Kaohsiung, Taiwan.

Publisher Item Identifier S 0018-9480(96)04725-4.

II. Theoretical Formulation

Fig. 1 shows the geometry under consideration. The inside cylindrical microstrip line [5], [6] is treated as a feed line, and the outside cylindrical microstrip line [7] is the coupled line. These two lines are assumed to be infinitely long and are coupled through a rectangular slot of dimensions $L \times W$ in the common cylindrical ground plane of radius b. The widths of the feed and coupled lines are $W_f(=2a\phi_f)$ and $W_c(=2c\phi_c)$, respectively. The feed substrate has a thickness h_f and a relative permittivity ε_f; the coupled substrate has a thickness h_c and a relative permittivity ε_c. The inner ($\rho < a$) and outer ($\rho > c$) regions are air with permittivity ε_0 and permeability μ_0. To begin with, we assume that the input power at port 1 is 1 watt and the microstrip lines are propagating quasi-TEM waves [2], [8]. And, by considering that the coupling slot is narrow ($L \gg W$), the electric field in the slot can be approximated as

$$\vec{E}^s = \hat{z} \sum_{q=1}^{N} V_q e_q^s(\phi, z) = \hat{z} \sum_{q=1}^{N} V_q \frac{1}{W} f_p^s(\phi - \phi_q), \quad |z| < \frac{W}{2}, \quad |\phi| < \phi_s \tag{1}$$

with

$$f_p^s(\phi) = \begin{cases} \dfrac{\sin k_e(b\phi_h - b|\phi|)}{\sin k_e b\phi_h}, & |\phi| < \phi_h, \\ 0, & |\phi| > \phi_h \end{cases}$$

$$\phi_q = \left[\frac{2q}{N+1} - 1\right]\phi_s,$$

$$\phi_h = \frac{2\phi_s}{N+1},$$

$$\phi_s = \frac{L}{2b},$$

$$k_e = k_0\sqrt{\frac{\varepsilon_f + \varepsilon_c}{2}},$$

$$k_0 = \omega\sqrt{\mu_0\varepsilon_0}$$

where $f_p^s(\phi)$ is a piecewise sinusoidal (PWS) basis function, ϕ_q is the center point of the qth expansion function, $b\phi_h$ is the half-length of the PWS function, and V_q is the unknown coefficient of the qth expansion function.

To solve for V_q, two boundary conditions are applied; one is the continuity of the tangential magnetic field at the slot position, and the other is that the tangential electric field must be zero on the coupled line. By considering the boundary condition that the tangential magnetic field must be continuous in the slot, we have

$$H_\phi^f + H_\phi^{sf} = H_\phi^c + H_\phi^{sc} \tag{2}$$

where H_ϕ^f and H_ϕ^c are, respectively, the fields contributed from the feed line and the coupled line in the absence of the slot; H_ϕ^{sf} and H_ϕ^{sc} are, respectively, the fields at $\rho = b^-$ and $\rho = b^+$ from the slot. By deriving the appropriate Green's functions for the cylindrical structure studied here, the magnetic fields in (2) can be expressed as

$$H_\phi^f = (1 - \Gamma)h_\phi^f \tag{3}$$

$$H_\phi^{sf} = \iint_{S_a} G_{\phi\phi}^{HMf}(b^-, \phi, z)M_\phi^{sf}\, ds_0 \tag{4}$$

$$H_\phi^c = \int_{-\infty}^{\infty}\int_{-W_c/2}^{W_c/2} G_{\phi z}^{HJc}(b^+, \phi, z)J_z^c\, ds_0 \tag{5}$$

$$H_\phi^{sc} = \iint_{S_a} G_{\phi\phi}^{HMc}(b^+, \phi, z)M_\phi^{sc}\, ds_0 \tag{6}$$

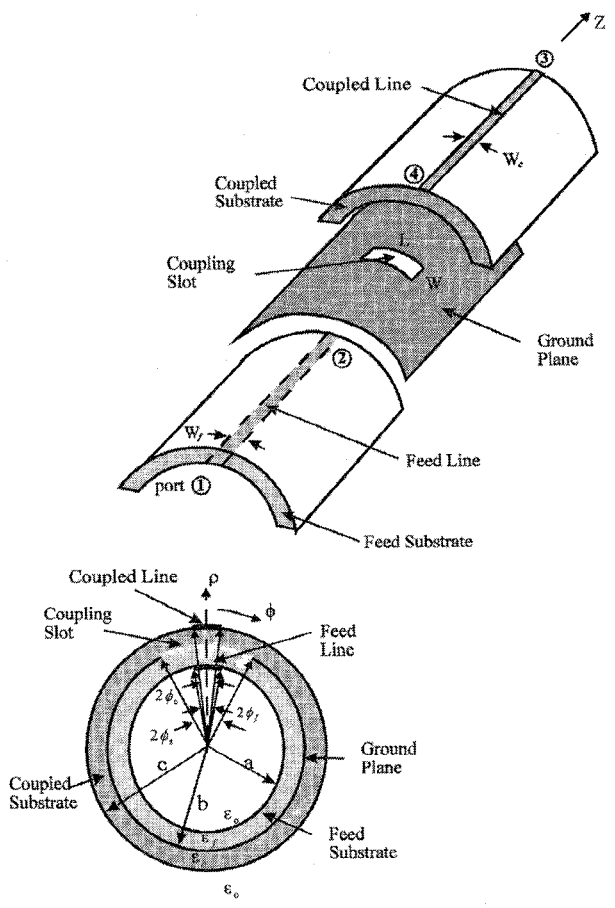

Fig. 1. The geometry of the slot-coupled double-sided cylindrical microstrip lines.

where Γ $(=S_{11})$ is the reflection coefficient on the feed line, h_ϕ^f is the normalized transverse magnetic field at the slot position caused by the feed line [8], J_z^c is the current density on the coupled line, and S_a is the slot area. M_ϕ^{sf} $(\vec{M}_\phi^{sf} = \hat{\phi} M_\phi^{sf} = -\hat{\rho} \times \vec{E}^s)$ and M_ϕ^{sc} $(=-M_\phi^{sf})$ are the equivalent magnetic currents at $\rho = b^-$ and $\rho = b^+$, respectively. $G_{\phi\phi}^{HMf}$, $G_{\phi z}^{IIJc}$, and $G_{\phi\phi}^{HMc}$ are Green's functions to account for the tangential magnetic field (H_ϕ) at the slot position due to M_ϕ^{sf}, J_z^c, and M_ϕ^{sc}, respectively. Multiplying (2) by the PWS functions and integrating over the slot area, we can obtain

$$([Y^{sf}] + [Y^{sc}])[V] = -(1-\Gamma)[\Delta v^f] + [\Delta v^c] \tag{7}$$

where $[Y^{sf}]$ and $[Y^{sc}]$ are the admittance matrices for the slot admittance looking at $\rho = b^-$ and $\rho = b^+$, respectively; $[V]$ is a coefficient matrix for V_q, $[\Delta v^f]$ is a matrix representing the voltage discontinuity across the slot, and $[\Delta v^c]$ denotes the reaction between the slot field and the current J_z^c. The expressions of the elements Y_{mq}^{sf} in $[Y^{sf}]$, Y_{mq}^{sc} in $[Y^{sc}]$, Δv_q^f in $[\Delta v^f]$, and Δv_q^c in $[\Delta v^c]$ are derived as

$$Y_{mq}^{s(f,c)} = \frac{2}{W^2\pi} \sum_{n=-\infty}^{\infty} \int_{-\infty}^{\infty} \frac{1}{k_z^2} \tilde{G}_{\phi\phi}^{HM(f,c)}(b, n, k_z) \cdot \sin^2\left(\frac{k_z W}{2}\right) \tilde{f}_p^{s^2}(n) \cos n(\phi_m - \phi_q)\, dk_z \tag{8}$$

$$\Delta v_q^f = \frac{-2}{\phi_f \beta_f W \sqrt{Z_{0f}}} \sum_{n=-\infty}^{\infty} \frac{1}{n} \tilde{G}_{\phi z}^{HJf}(b, n, -\beta_f) \cdot \sin n\phi_f \sin\left(\frac{-\beta_f W}{2}\right) \tilde{f}_p^s(n) \cos n\phi_q \tag{9}$$

$$\Delta v_q^c = -\frac{1}{W\pi} \sum_{n=-\infty}^{\infty} \int_{-\infty}^{\infty} \frac{1}{k_z} \tilde{G}_{\phi z}^{HJc}(c, n, k_z) \cdot \tilde{J}_z^c \sin\left(\frac{k_z W}{2}\right) \tilde{f}_p^s(n) \cos n\phi_q\, dk_z \tag{10}$$

with

$$\tilde{f}_p^s(n) = \frac{2k_e(\cos n\phi_h - \cos k_e b\phi_h)}{\left[k_e^2 - \left(\frac{n}{b}\right)^2\right] \sin k_e b\phi_h}$$

where Z_{0f} and β_f are, respectively, the characteristic impedance and propagation constant of the feed line [5]; the tilde denotes a Fourier transform; $G_{\phi z}^{HJf}$ is a Green's function for H_ϕ at the slot position due to J_z^f, the current density on the feed line.

As for the second boundary condition that the electric field on the coupled line must vanish, we can derive

$$\int_{-\infty}^{\infty} \int_{-W_c/2}^{W_c/2} G_{zz}^{EJc}(c, \phi, z) J_z^c\, ds_0 + \iint_{S_a} G_{z\phi}^{EMc}(c, \phi, z) M_\phi^{sc}\, ds_0 = 0 \tag{11}$$

where G_{zz}^{EJc} and $G_{z\phi}^{EMc}$ are the Green's functions showing the tangential electric field (E_z) on the coupled line due to J_z^c and M_ϕ^{sc}, respectively. By assuming that the coupled line also propagates a quasi-TEM mode, J_z^c can be expressed as [2]

$$J_z^c(\phi, z) = \begin{cases} I_0 \dfrac{1}{W_c} e^{-j\beta_c z}, & z > 0 \\ I_0 \dfrac{1}{W_c} e^{j\beta_c z}, & z < 0 \end{cases} \tag{12}$$

where β_c is the propagation constant of the coupled line, I_0 is the unknown current amplitude coupled from the feed line, and a pulse function $(1/W_c)$ is assumed for the ϕ dependence. Then, by following a similar theoretical treatment described in [2] for (11), we can obtain a relationship between I_0 and V_q; that is

$$ZI_0 + [V]^t[N^s] = 0 \tag{13}$$

with

$$Z = -\frac{1}{2\pi} \sum_{n=-\infty}^{\infty} \tilde{G}_{zz}^{EJc}(c, n, -\beta_c) \frac{\sin^2 n\phi_c}{(n\phi_c)^2} \tilde{f}_p^c(-\beta_c)$$

$$N_q^s = \frac{1}{W\phi_c\pi} \sum_{n=-\infty}^{\infty} \int_{-\infty}^{\infty} \frac{1}{k_z n} \tilde{G}_{z\phi}^{EMc}(c, n, k_z) \cdot \sin\left(\frac{k_z W}{2}\right) \sin n\phi_c \tilde{f}_p^s(n) \tilde{f}_p^c(k_z) \cos n\phi_q\, dk_z$$

$$\tilde{f}_p^c(k_z) = \frac{2k_e(\cos k_z h - \cos k_e h)}{(k_e^2 - k_z^2) \sin k_e h}$$

where $[V]^t$ is the transpose of $[V]$ and N_q^s is the element in $[N^s]$.

By substituting the Fourier transform of (12) into (10) and applying the reciprocity relationship of $\tilde{G}_{\phi z}^{HJc} = -c\tilde{G}_{z\phi}^{EMc}/b$ [8], the element Δv_q^f can be derived as

$$\Delta v_q^c = I_0 \cdot N_q^c \tag{14}$$

where

$$N_q^c = \frac{c}{W\beta_c\phi_c\pi b} \sum_{n=-\infty}^{\infty} \frac{1}{n} \tilde{G}_{z\phi}^{EMc}(c, n, -\beta_c) \cdot \sin n\phi_c \sin\left(\frac{-\beta_c W}{2}\right) \tilde{f}_p^s(n) \cos n\phi_q.$$

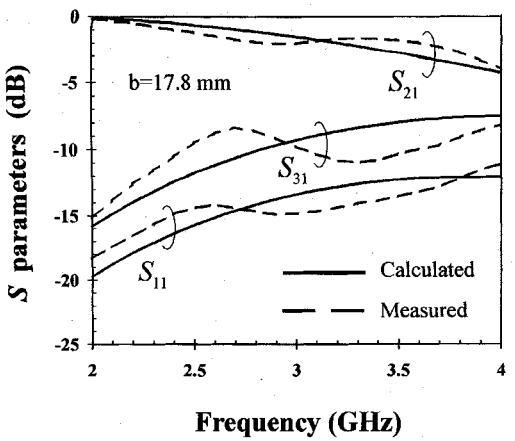

Fig. 2. Calculated and measured S parameters for the slot-coupled double-sided cylindrical microstrip lines; b = 17.8 mm, $\varepsilon_f = \varepsilon_c$ = 3.0, $h_f = hc$ = 0.762 mm, L = 15 mm, W = 1.0 mm, $W_f = W_c$ = 1.9 mm.

Rewriting (14) in the matrix form as $[\Delta v^c] = I_0[N^c]$ and substituting it into (7), we get

$$([Y^{sf}] + [Y^{sc}] + [Y^c])[V] = -(1 - \Gamma)[\Delta v^f] \tag{15}$$

where

$$[Y^c] = \frac{[N^s][N^c]^t}{Z}.$$

With the reflection coefficient Γ expressed as [2], [8]

$$\Gamma = \frac{-[V]^t[\Delta v^f]}{2} \tag{16}$$

the $[V]$ matrix for the slot field can be easily calculated from (15). And the coupling coefficient S_{31}, defined as the power ratio between port 3 and port 1, can then be evaluated from

$$S_{31} = |I_0|\sqrt{Z_{0c}} = \frac{-[V]^t[N^s]\sqrt{Z_{0c}}}{Z} \tag{17}$$

where Z_{0c} is the characteristic impedance of the coupled line [7].

III. Results and Conclusion

Fig. 2 shows the calculated and measured S parameters versus frequency for the slot-coupled cylindrical microstrip lines. The calculated results are obtained using three ($N = 3$) PWS basis functions for the expansion of the slot field, which ensures good numerical convergence. For the experiment, several slot-coupled cylindrical microstrip lines were constructed, and a network analyzer (HP8510C) was used for the measurement. The characteristic impedances of the feed and coupled lines were both designed to be 50 Ω in the planar geometry, and 50 Ω terminators were connected at ports 3 and 4 for measuring S_{11} and S_{21}. For measuring S_{31}, both ports 2 and 4 were connected to 50 Ω terminators. It is seen that the calculated results in general agree with the measured data except for some ripples appearing in the measured data. These ripples are probably due to the shifting of the characteristic impedances (Z_{0f} and Z_{0c}) of the inside and outside cylindrical microstrip lines away from 50 Ω [5]–[7], which results in a mismatch of the microstrip lines to the 50 Ω terminators.

Fig. 3 presents the variations of the S parameters as a function of the coupling slot length for different cylinder radii. It is seen that the reflection coefficient, S_{11}, increases with increasing cylinder radius, and the transmission coefficient, S_{21} (=1 − Γ), and coupling coefficient, S_{31}, decrease with increasing cylinder radius. The S parameters are also greatly affected by the coupling slot length.

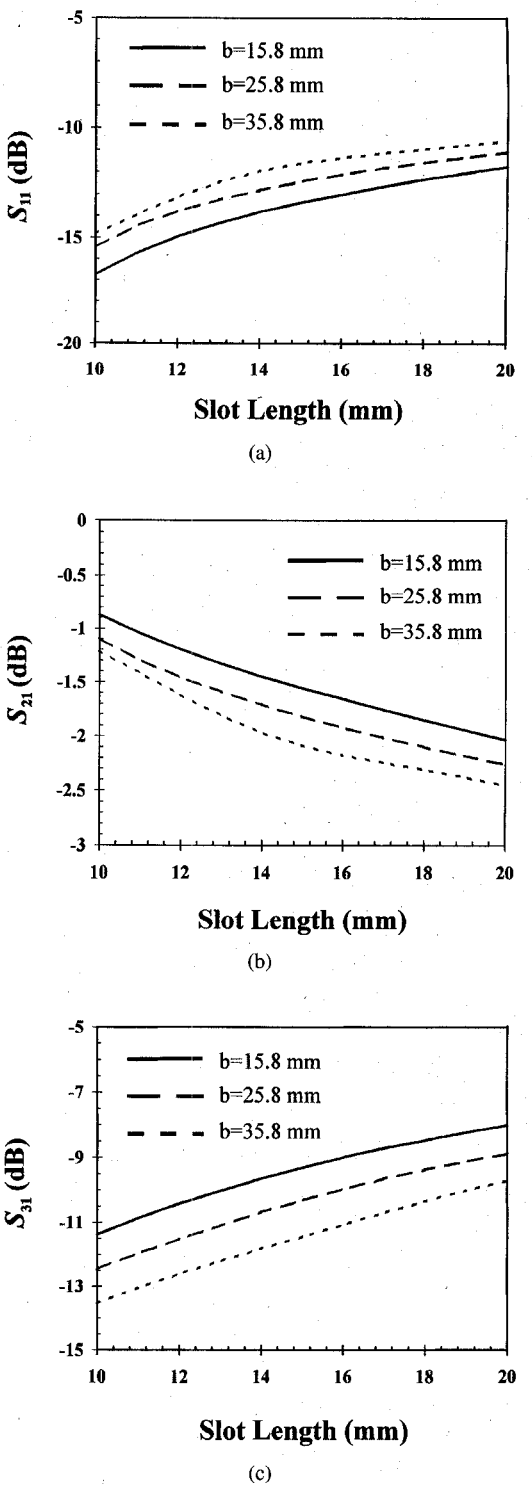

Fig. 3. Calculated S parameters for the slot-coupled double-sided cylindrical microstrip lines with a cylindrical radius of b = 15.8, 25.8, and 35.8 mm; f = 3 GHz. Other parameters are the same as given in Fig. 2. (a) S_{11}, (b) S_{21}, and (c) S_{31}.

In summary, characteristics of slot-coupled double-sided cylindrical microstrip lines have been studied. The S parameters have been formulated and calculated. Theoretical results are verified by the measurements, and the S parameters are seen to be significantly affected by the coupling slot length and the curvature of the cylindrical ground plane.

REFERENCES

[1] T. Tanaka, K. Tsunoda, and M. Aikawa, "Slot-coupled directional couplers between double-sided substrate microstrip lines and their applications," *IEEE Trans. Microwave Theory Tech.*, vol. 36, pp. 1752–1757, Dec. 1988.

[2] N. Herscovici and D. M. Pozar, "Full-wave analysis of aperture-coupled microstrip lines," *IEEE Trans. Microwave Theory Tech.*, vol. 39, pp. 1108–1114, July 1991.

[3] M. F. Wong, V. F. Hanna, O. Picon, and H. Baudrand, "Analysis and design of slot-coupled directional couplers between double-sided substrate microstrip lines," *IEEE Trans. Microwave Theory Tech.*, vol. 39, pp. 2123–2129, Dec. 1991.

[4] C. Wan, "Quasistatic analysis of slot-coupled double-sided microstrip lines by conformal mapping," *Microwave Opt. Technol. Lett.*, vol. 9, pp. 253–256, Aug. 5, 1995.

[5] R. B. Tsai and K. L. Wong, "Characterization of cylindrical microstriplines mounted inside a ground cylindrical surface," *IEEE Trans. Microwave Theory Tech.*, vol. 43, pp. 1607–1610, July 1995.

[6] ——, "Quasistatic solution of a cylindrical microstripline mounted inside a ground cylinder," *Microwave Opt. Technol. Lett.*, vol. 8, pp. 136–138, Feb. 20, 1995.

[7] N. G. Alexopoulos and A. Nakatani, "Cylindrical substrate microstrip line characterization," *IEEE Trans. Microwave Theory Tech.*, vol. 35, pp. 843–849, Sept. 1987.

[8] R. B. Tsai, "Analysis of cylindrical printed slot and slot-coupled microstrip antennas," Ph.D. dissertation, Dept. of Electrical Eng., National Sun Yat-Sen Univ., Kaohsiung, Taiwan, June 1995.

Substrate Parasitics and Dual-Resistivity Substrates

Rex Lowther, Patrick A. Begley, George Bajor,
Anthony Rivoli, and William R. Eisenstadt

***Abstract*—In high-frequency semiconductor applications, substrate effects can be a dominant source of parasitics unless they are carefully minimized. Here a dual-resistivity substrate in a bonded-oxide process is considered for the optimization of the two major types of substrate parasitics: resistive substrate losses and capacitive coupling (crosstalk) through the substrate. These will both depend on the frequency, the two substrate resistivities, and the thickness of the two substrate layers. The thickness of the upper layer is treated as a fully designable parameter. The mechanisms will be evaluated numerically, but intuitive rule-of-thumb arguments will also be provided for a good understanding of the physics and of the tradeoffs in selecting an optimal design. The results of these sections may also serve as a guide for determining standard substrate resistivities.**

I. INTRODUCTION

Integrated circuits that operate at microwave frequencies are implemented on substrates comprising monocrystalline gallium arsenide or by using hybrid circuit techniques. These technologies are effective in producing integrated circuits operating at microwave frequencies, but they still have several drawbacks. Both technologies can be expensive and generally produce circuits of low device density compared to the cost and density of devices in planar silicon integrated circuits. Attempts to implement microwave frequency integrated circuits with conventional silicon technology have been limited due to high losses occurring in the silicon substrate at gigahertz frequencies [1]. These lossses lower transistor performance and also greatly lower the Q factor of integrated silicon inductors and capacitors. Highly resistive float-zone silicon substrates (HRS), however, have been shown to limit these losses nearly as well as GaAs and these have also been successfully applied at multigigahertz frequencies [1]–[5]. Unfortunately, these substrates are very expensive and are limited in wafer diameter to 100 mm. A dual-substrate structure, analyzed herein, describes a bonded-wafer process that has resistive substrate losses nearly as low as HRS, and lower cross-talk than HRS—while retaining the much lower cost of conventional bonded wafers.

Manuscript received August 28, 1995; revised March 20, 1996.

R. Lowther, P. A. Begley, G. Bajor, and A. Rivoli are with Harris Semiconductor, Melbourne, FL USA.

W. R. Eisenstadt is in the Department of Electrical Engineering and Computer Science, University of Florida, Gainesville, FL USA.

Publisher Item Identifier S 0018-9480(96)04726-6.

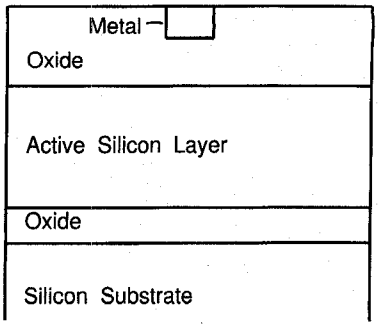

Fig. 1. Cross-section of a typical SOI geometry.

In the next section, resistive losses from induced current are analyzed and estimated for both standard and dual-resistivity substrates. The simple, but illustrative, and worst-case example of a long, straight metal line is used to get an estimate of these losses. The two following sections analyze capacitive coupling of nearby devices through the substrate for both standard substrates and the proposed dual substrates, respectively. Finite-difference device simulation is used to obtain an understanding of, and estimates of, the cross-talk. In the "process" section, the most likely method for making such a structure is discussed. Finally, design examples are chosen to illustrate the tradeoffs in the substrate parameters, and the comparative value of the dual-resistivity substrate structure to standard highly resistive substrates is discussed.

II. SUBSTRATE RESISTIVE LOSSES

Consider first the worst-case example of a very long, straight metal line running over various layers as shown in cross section in Fig. 1. In nearly all practical cases, induced current in the active silicon layer can be ignored because it is thin compared with its own skin depth for most typical doping levels and because areas of high doping are usually confined, isolated regions too small to allow significant conduction. The active silicon region therefore can be considered to be an insulator for this parasitic—allowing the device layer and the two oxide layers in Fig. 1 to be treated as a single insulator.

Assume for now a uniform substrate with resistivity low enough that the skin depth is much less than the substrate thickness. For distances more than a few skin depths below the substrate-insulator interface, it is known that both the electric and magnetic fields due to ac current are essentially zero. Therefore the sum effect of the induced electric field is to generate current such that it is equal in magnitude and opposite in direction to the ac current in the metal line. This is simply return current in a ground plane. At microwave